nature communications

Article

https://doi.org/10.1038/s41467-024-51332-7

Clinical utility of a blood based assay for the detection of IDH1.R132H-mutant gliomas

Received: 9 February 2024

Accepted: 5 August 2024

Published online: 16 August 2024

Check for updates

Syeda Maheen Batool[1], Ana K. Escobedo[1], Tiffaney Hsia[1], Emil Ekanayake[1], Sirena K. Khanna[1], Austin S. Gamblin[1], Hui Zheng[2], Johan Skog[3], Julie J. Miller[4,5], Anat O. Stemmer-Rachamimov[6], Daniel P. Cahill[1], Leonora Balaj[1,7] & Bob S. Carter[1,7]

Glioma represents the most common central nervous system neoplasm in adults. Current classification scheme utilizes molecular alterations, particularly IDH1.R132H, to stratify lesions into distinct prognostic groups. Identification of the single nucleotide variant through traditional tissue biopsy assessment poses procedural risks and does not fully reflect the heterogeneous and evolving tumor landscape. Here, we introduce a liquid biopsy assay, *mt*-IDH1$_{dx}$. The blood-based test allows minimally invasive detection of tumor-derived extracellular vesicle RNA using only 2 ml plasma volume. We perform rigorous, blinded validation testing across the study population ($n = 133$), comprising of IDH1.R132H patients ($n = 80$), IDH1 wild-type gliomas ($n = 44$), and age matched healthy controls ($n = 9$). Results from our plasma testing demonstrate an overall sensitivity of 75.0% (95% CI: 64.1%–84.0%), specificity 88.7% (95% CI: 77.0%–95.7%), positive predictive value 90.9%, and negative predictive value 70.1% compared to the tissue gold standard. In addition to fundamental diagnostic applications, the study also highlights the utility of *mt*-IDH1$_{dx}$ platform for blood-based monitoring and surveillance, offering valuable prognostic information. Finally, the optimized workflow enables rapid and efficient completion of both tumor tissue and plasma testing in under 4 hours from the time of sampling.

Glioma is the most common primary central nervous system (CNS) neoplasm in adults with an overall incidence of 6 cases per 100,000 people in the US every year[1]. The 2021 WHO classification of brain tumors provides a new framework for comprehensive characterization of gliomas based on histology and independently by hallmark molecular alterations. Importantly, IDH1 mutant alteration represents a key diagnostic biomarker, prevalent in >80% of WHO grade II/III gliomas[2], >70% of Secondary Glioblastoma (GBM)[3], and <10% of Primary GBM[4] (all previous IDH1 mutant GBM lesions are now classified as Grade 4, Astrocytoma). This point mutation is found in codon 132, characterized by G>A transition (CGT>CAT) at nucleotide position 395, resulting in the substitution of arginine for histidine[3]. IDH1 mutant gliomas represent a distinctive subtype with important clinical implications, most importantly improved prognosis and survival outcomes[5].

Currently, neuroimaging followed by tissue biopsy testing (surgical biopsy and/or resection) is the current gold standard modality for diagnosing IDH1 mutant gliomas[6]. A range of testing platforms are used with varying sensitivity and depth of coverage and include

[1]Department of Neurosurgery, Massachusetts General Hospital, Harvard Medical School, Boston, MA, USA. [2]Center for Biostatistics, Massachusetts General Hospital, Harvard Medical School, Boston, MA, USA. [3]Exosome Diagnostics, a Bio-Techne Brand, Waltham, MA, USA. [4]Translational Neuro-Oncology Laboratory, Massachusetts General Hospital, Harvard Medical School, Boston, MA, USA. [5]Center for Neuro-Oncology, Department of Neurology, Massachusetts General Hospital, Harvard Medical School, Boston, MA, USA. [6]Department of Pathology, Massachusetts General Hospital, Harvard Medical School, Boston, MA, USA. [7]These authors jointly supervised this work: Leonora Balaj, Bob S. Carter. e-mail: balaj.leonora@mgh.harvard.edu

immunohistochemistry (IHC), DNA-based PCR, and Next Generation Sequencing (NGS)[7]. The turnaround time for diagnosis from the point of intraoperative sampling is around 2–3 weeks. Furthermore, in addition to being invasive, surgical tissue biopsy relies on spatial sampling (lesion edge, core) and availability of sufficient and adequate tissue[8]. Finally, tissue biopsy can not be readily repeated in longitudinal settings for disease surveillance and treatment monitoring. This serves as a major limitation in tracking the dynamic, evolving molecular profile secondary to treatment, surgical intervention, and/or natural disease progression. Furthermore, a recent study has also reported a detrimental effect on overall survival of tumor tissue biopsy over "upfront resection" in high-grade gliomas[9].

Liquid biopsy, defined as sampling and analysis of biofluids (plasma, cerebrospinal fluid, urine, saliva) has emerged as a promising platform for rapid, minimally invasive diagnosis of a range of cancers including gliomas[10–12]. This is achieved by isolation and downstream analysis of a range of circulating tumor-tissue-derived analytes closely reflecting the epitranscriptome profile of tumor cell of origin: extracellular vesicles (EVs), circulating tumor cells (CTCs), cell-free DNA (cfDNA), and circulating RNA. Our group has previously optimized and developed highly sensitive (>75%) and specific (>90%) blood and CSF-based assays for the detection of pivotal DNA (TERT C228T/C250T[13]) and RNA (EGFRvIII[14,15]) based alterations prevalent in different glioma subtypes.

Expanding our efforts to IDH1.R132H detection, we have previously utilized the technology of BEAMing (beads, emulsion, amplification, magnetics) PCR for reliable detection of IDH1.R132H mutant EV RNA transcripts in CSF of patients with gliomas[16]. Here, we show a Droplet Digital PCR (ddPCR) assay, called *mt*-IDH1$_{dx}$, for robust detection of IDH1.R132H in patient plasma derived EV RNA. To evaluate the assay performance in our study population ($N = 133$), we perform blinded validation testing across three independent cohorts. Baseline Plasma testing from IDH1.R132H patients ($n = 80$), IDH1 wild-type gliomas ($n = 44$), and age matched healthy controls ($n = 9$) demonstrates clinically relevant diagnostic sensitivity and specificity. Finally, we show the utility of the proposed blood-based in longitudinal disease monitoring and surveillance in ($n = 8$) patients with IDH1.R132H alteration.

Results

Detection of IDH1.R132H mutation via RNA yields higher sensitivity compared to DNA-based methods

The canonical alteration in IDH1 mutant glioma, IDH1.R132H (IDH1mt) mutation occurs as a result of G>A transition at nucleotide position 395, in the tail region of exon 4 with close proximity to the exon 5 nucleotide region (Supplementary Fig. 1a). This unique location allows possible variant detection in both DNA and RNA. To investigate the contribution of IDH1mt signal in both RNA and DNA in different sample types, we designed and optimized both DNA (amplicon size, 49 bp) and RNA (amplicon size, 62 bp) based assays (Supplementary Fig. 1a). Four different combinations of Mutant and Wild-type probes were tested to achieve optimal signal separation in 1-D and 2-D amplitude plots with minimal cross-reactivity of the two probes (Supplementary Fig. 1b–c). The final assays were then utilized for direct DNA vs RNA IDH1mt signal comparison.

First, we extracted DNA and RNA from IDH1.R132H mutant tumor tissue of one patient (described in Methods). Both analytes were diluted to yield a wide range of DNA/RNA inputs (30.0–0.3 ng; Fig. 1a). IDH1.R132H mutant allele frequency (MAF, %) measured across all concentrations was significantly ($p < 0.0001$, ****) higher in RNA (34.40%, 95% CI; 32.69–36.11%) as compared to DNA (12.31%, 95% CI; 11.09–13.53%) from the same specimen (Fig. 1a). Next, we compared the RNA/DNA enrichment ratio in a tumor tissue cohort ($n = 23$) of different IDH1mt glioma subtypes; Astrocytoma, Grade 2–3 ($n = 12$), Oligodendroglioma, Grade 2–3 ($n = 7$), and Astrocytoma, Grade 4 ($n = 4$) (Fig. 1b). We again observed a significantly higher enrichment of IDH1.R132H MAF in RNA compared to DNA across all glioma subtypes (Fig. 1b), with the highest RNA/DNA enrichment in oligodendrogliomas followed by high grade and low grade astrocytomas (Average fold change, 8.5, 5.6 and 2.8 respectively) (Fig. 1b). Finally, we investigated the spatial variation of RNA/DNA enrichment ratio within different regions of tumor lesion (Fig. 1c). A total of $n = 3$ patients (oligodendroglioma = 2, astrocytoma = 1) and 12 regions (4 per patient) were analyzed. Again, on average, spatial analysis of oligodendrogliomas demonstrated 22-fold RNA/DNA enrichment (95% CI: 13.49–30.97%) as compared to 2.5-fold change in astrocytomas (95% CI: 1.36–3.62%) (Fig. 1c).

Extending this comparison to biofluids, we tested 5 plasma samples consisting of IDH1.R132H mutant patients ($n = 3$) and healthy controls ($n = 2$). Parallel processing of 2 ml was performed to isolate either i) EV RNA (ExoLution™, see Methods), or ii) EV RNA + EV DNA + cfDNA (ExoLutionPlus™, see Methods). There was a striking difference in the downstream ddPCR (see Methods) detection of IDH1.R132H (Fig. 1d, left panel) and IDH1 wild-type signals (Fig. 1d, right panel), with the detection of mutant signals in all three patients using EV RNA analyte. However, no IDH1.R132H signal was detected using the DNA-based approach (Fig. 1d, top panel) in addition to yielding a significantly lower IDH1 wild-type signal (IDH1wt) in patients and controls (Fig. 1d, bottom panel).

We next optimized downstream Reverse transcription (Supplementary Fig. 2e) and Droplet digital PCR (ddPCR) conditions (annealing temperature, preamplification supermix; Supplementary Fig. 2a–e). In order to improve sensitivity in low input plasma samples, three different preamplification conditions were tested using 1.0 ng RNA input: (i) Forward and Reverse primers only, (ii) Primers + Mutant probe + Wild-type probe, (ii) Primers and Mutant probe (Fig. 1e). Highest IDH1.R132H MAF was seen with condition (iii) with the difference being statistically significant. Next, the optimal preamplification condition was tested using IDH1 wild-type tumor tissue (RNA, 2 ng) and healthy control plasma (2 ml) with and without the presence of a previously designed wild-type blocker (see Methods, Supplementary Fig. 2f) at an optimized concentration (Supplementary Fig. 2f). The presence of wild-type blocker during preamplification facilitated the elimination of false positive signals in both control samples, thereby improving signal-to-noise ratio (Fig. 1f). Similar testing also demonstrated a favorable effect in reducing the IDH1wt signal in IDH1.R132H mutant plasma samples (Supplementary Fig. 2f).

The optimized ddPCR assay (hereinafter termed *mt*-IDH1$_{dx}$ assay) was tested to determine linearity and limit of detection (LOD)/Limit of Blank (LOB). A range of different concentrations of IDH1.R132H RNA (10.0–0.02) ng were spiked into a constant IDH1 wild-type background RNA (10.0 ng) prior to reverse transcription (Fig. 1g, h). The final ddPCR was performed in three replicates at each concentration. A linear trend was observed in the IDH1.R132H signal with an R^2 of 0.99, LOD of 0.06%, and LOB of 0.02% (Fig. 1g, h).

mt-IDH1$_{dx}$ assay testing in IDH1.R132H mutant tumor tissue demonstrates diagnostic and prognostic utility

As current glioma tumor biopsy to determine IDH1mt status is invasive, time intensive, costly, and frequently lacks sensitivity, we then tested the proposed *mt*-IDH1$_{dx}$ assay (Fig. 1) in a variety of clinical samples to assess assay performance in both tissue and biofluids and compared these results to clinically reported results (Fig. 2a).

The *mt*-IDH1$_{dx}$ assay performance was first evaluated in a cohort of tumor tissue ($n = 48$; Fig. 2b) consisting of astrocytomas, grade 2–3 ($n = 25$), oligodendrogliomas, grade 2–3 ($n = 11$), and astrocytomas, grade 4 ($n = 12$). The IDH1mt status was determined by MGH clinical pathology in astrocytomas, grade 2–3 ($n = 21$), oligodendrogliomas, grade 2–3 ($n = 11$), and astrocytomas, grade 4 ($n = 7$) (Fig. 2b) and confirmed by the *mt*-IDH1$_{dx}$ assay (100% concordance) (Fig. 2c–e).

Interestingly, the *mt*-IDH1$_{dx}$ assay also detected the IDH1mt signal in an additional subset of Grade 2–3, Astrocytomas ($n = 2$, Fig. 2c) and

https://doi.org/10.1038/s41467-024-51332-7

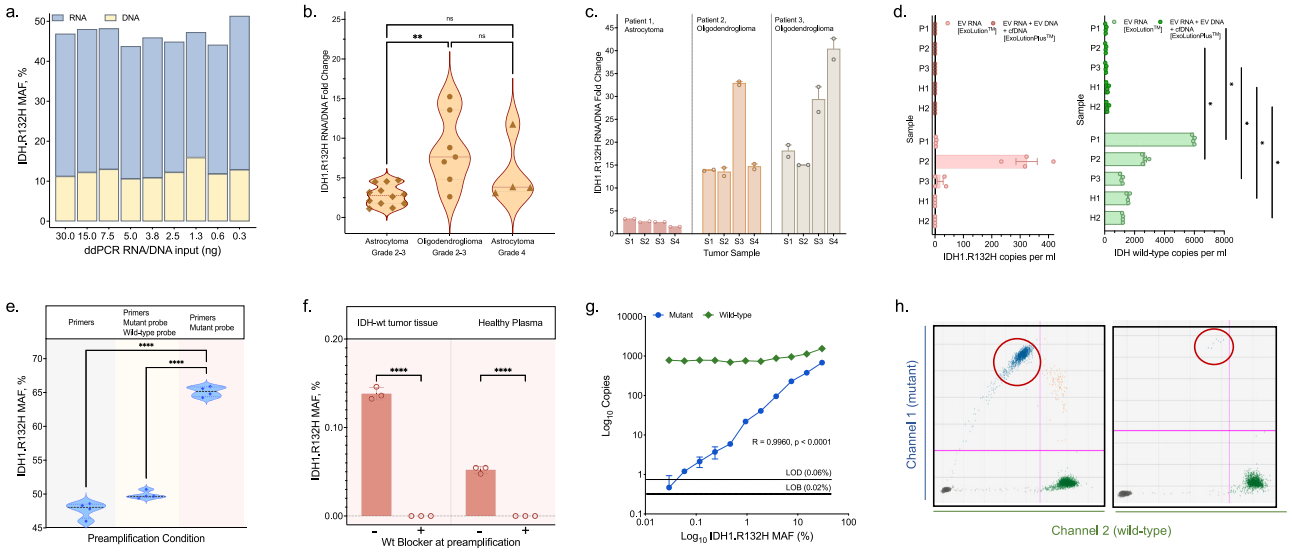

Fig. 1 | RNA-based approach enables higher sensitivity of mutation analysis compared to DNA-based detection. Multi-phase testing of IDH1.R132H, Mutant Allele Frequency (MAF, %) enrichment in RNA versus DNA: (**a**) Stacked Graph depicting IDH1.R132H MAF % (average of three replicates) in tumor tissue ($n = 1$) derived RNA/DNA in a range equal ddPCR inputs (30.0–0.30) ng, (**b**) Violin plot comparing IDH1.R132H MAF, % RNA vs DNA Fold-Change (FC = RNA, MAF%/DNA, MAF%) across three glioma subtypes (Astrocytoma, Grade 2–3; $n = 12$, Oligodendroglioma, Grade 2–3; $n = 7$, Astrocytoma, Grade 4; $n = 4$). Each data point represents an individual patient (average of three technical replicates). Average FC was compared across the groups using one-way ANOVA (alpha 0.05, Tukey's multiple comparisons). Results of mean difference across multiple comparisons: Astrocytoma, Grade 2, 3 vs. Oligodendroglioma, Grade 2, 3 (−5.718, $p = 0.0025$), Astrocytoma, Grade 2, −3 vs Grade 4 (−2.828, $p = 0.2749$), and Oligodendroglioma vs Astrocytoma, Grade 4 (2.889, $p = 0.3159$). **c** Bar-graph depicting the spatial variation in IDH1.R132H MAF, % RNA vs DNA Fold-Change (mean ± SEM) in spatial (multi-region; core, edge) samples analyzed from astrocytoma ($n = 1$) and oligodendroglioma ($n = 2$)., and (**d**) Sensitivity of IDH1.R132H (left, mean ± SEM; 4 replicates) and IDH1 wild-type (right, mean ± SEM; 4 replicates) detection in a cohort ($n = 5$) of 2 ml plasma-derived EV RNA (ExoLution™) versus EV RNA + EV DNA + cfDNA (ExoLutionPlus™). Results of IDH1.R132H copy number (left) showed no detection in P1-P3 and H1-H2 using ExoLutionPlus™. For P1-P3 the bars denote mean ± SEM (P1; 3.081, 95% CI: 1.072–5.090, P2: 322.849, 95% CI: 203.57–422.341, P3: 18.091, 95% CI: −15.345–51.526). Multiple unpaired t tests were performed to compare the difference in IDH1 wild-type copy number (right) across the individual patients (P1–P3) and controls (H1–H2). Across all individual patients and controls, p value < 0.000001 when comparing mean differences (mean ± SEM): (P1; 5876 ± 44.43, P2: 2619 ± 109.6, P3: 1064 ± 49.41, H1: 1382 ± 60.72, H2: 1018 ± 40.54). **e** Violin plot depicting variation of IDH1.R132H MAF % across three different optimization conditions (4 technical replicates per condition) of preamplification PCR. Average MAF % was compared across the groups using one-way ANOVA (alpha 0.05, Tukey's multiple comparisons). Results of mean difference across multiple comparisons: Primers vs. (Primers + Mutant Probe) (−17.46, p value < 0.0001), Primers vs (Primers + Mutant, Wild-type Probe) (−2.191, p value 0.0145), and (Primers + Mutant Probe) vs (Primers + Mutant, Wild-type Probe) (15.27, p value < 0.0001). **f** Preamplification of IDH1 wild-type tumor tissue and healthy plasma with (+, 3 technical replicates) and without (−, 3 technical replicates) the presence of an optimized wild-type blocker to compare the false positive signal. Results plotted as a bar graph (mean ± SEM). Average MAF % was compared across the groups using one-way ANOVA (alpha 0.05, Sidak's multiple comparisons). Results of mean difference across multiple comparisons: Wild-type tumor tissue, no blocker vs. blocker (0.1381, p value < 0.0001), Healthy Plasma, no blocker vs blocker (0.0522, p value < 0.0001). **g** Assessment of optimized Droplet Digital PCR (ddPCR) assay linearity and determination of Limit of Detection (LOD) and Limit of Blank (LOB). At each input concentration, $n = 3$ technical replicates were run at the ddPCR step. Each data point on the line graph denotes Mean ± SEM, 3 technical replicates. **h** 2-D ddPCR plots of highest and lowest IDH1.R132H MAF, % detected. Source Data are provided as a Source Data file.

Grade 4, Astrocytomas ($n = 4$, Fig. 2d) lesions that were classified as IDH1.R132H wt by MGH clinical pathology. The low grade astrocytomas were classified as IDH1.R132C and IDH1.R132S mutant by histopathology testing.

Distribution analysis of the IDH1mt copies (Fig. 2f), IDH1wt copies (Fig. 2g), and IDH1.R132H MAF (Fig. 2h) in tumor tissue suggested a significantly higher IDH1mt expression level in oligodendrogliomas (mean 1926 ± 1373 copies, 95% CI: 1004–2848) followed by astrocytomas, grade 4 (mean: 963 ± 1716 copies, 95% CI: 963–2053) and astrocytomas, grade 2–3 (mean 698 ± 672 copies, 95% CI: 420–975) (Fig. 2f). IDH1wt was found to be highly overexpressed in grade 4 astrocytoma (Glioblastoma, based on previous WHO classification) tumor tissue (mean 3404 ± 3351 copies, 95% CI: 1275–5534), as compared to low grade astrocytomas (mean 1436 ± 844) and oligodendrogliomas (mean 2125 ± 1200) (Fig. 2g). Finally, IDH1.R132H MAF reflecting mutational expression, was highest in oligodendrogliomas tumors (mean: 44.5% ± 12.6, 95% CI: 36.0–52.9%), followed by low grade astrocytomas (mean: 27.2% ± 16.3, 95% CI: 20.1–33.9%) and high-grade astrocytomas (mean: 20.4% ± 20, 95% CI: 7.7–33.1%) (Fig. 2h).

Following signal quantification in the different clonal subtypes, Kaplan–Meier analysis was performed to compare the overall prognosis in patients with different patterns of IDH1mt detection. Median Overall Survival (OS) was determined to be highest in the oligodendroglioma subtype (132.8 months) followed by grade 2–3, astrocytoma (101.5 months) and grade 4, astrocytoma subtype (52.6 months; Fig. 2i). Correlation of the OS to MAF distribution (Fig. 2h), demonstrated a positive correlation of tissue IDH1.R132H MAF with overall survival, with highest tumor tissue IDH1.R132H MAF in oligodendrogliomas also associated with highest overall survival. Similarly, the subtype with lowest MAF (astrocytoma, grade 4) indicated significantly shorter overall survival. To investigate this relationship further, we stratified the patient population into two groups based on ddPCR derived IDH1.R132H tissue MAF cut-off (≤38%, >38%; Fig. 2j) determined by the overall distribution in the population. Importantly, this analysis also demonstrated a survival benefit in the group with higher IDH1.R132H MAF (>38%) with approximately 2-fold higher median OS (130.1 months) compared to the group with lower MAF (≤38%: 75.8 months) (Fig. 2j). Additional IDH1.R132H MAF correlative

https://doi.org/10.1038/s41467-024-51332-7

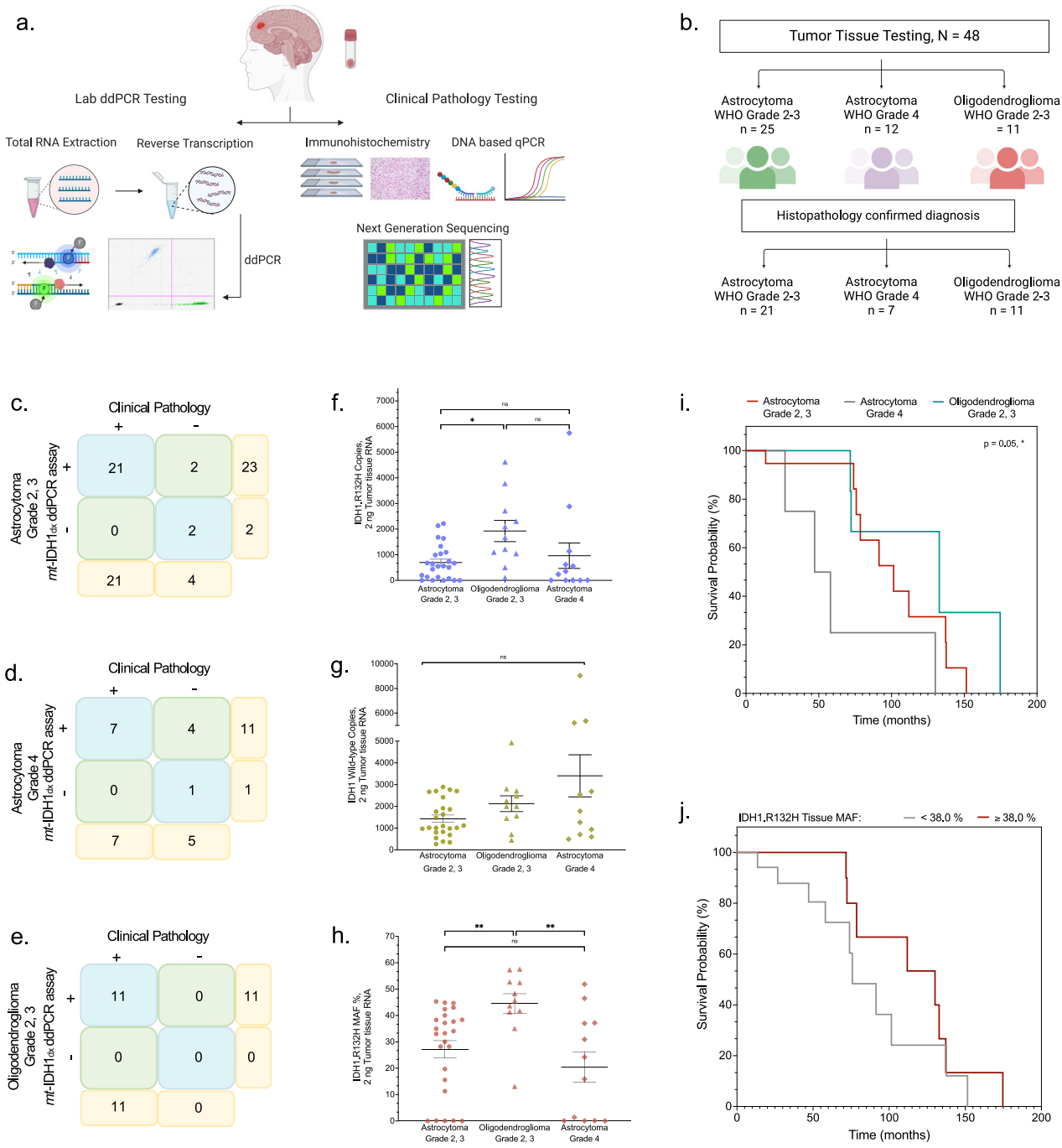

Fig. 2 | Enhanced performance of the *mt*-IDH1$_{dx}$ assay in tumor tissue across the glioma subtypes. a Schematic comparing the modalities routinely applied in clinical settings for determination of IDH1.R132H status versus the one-step laboratory developed Droplet Digital PCR platform, referred to as *mt*-IDH1$_{dx}$ ddPCR assay, for rapid, tumor tissue diagnostics. **b** *mt*-IDH1$_{dx}$ assay performance evaluated in tumor tissue cohort ($N = 48$) in comparison to clinical pathology testing across different histological subtypes: (**c**) Astrocytoma, Grade 2, 3 ($n = 25$, biological replicates), (**d**) Astrocytoma, Grade 4 ($n = 12$, biological replicates), and (**e**) Oligodendroglioma, Grade 2, 3 ($n = 11$, biological replicates). **f**–**h** Astrocytomas, Grade 4 category includes $n = 3$ GBM tumor tissue samples that were determined IDH1 mutant by the ddPCR assay. **f**–**h** Scatter-dot plots demonstrating the overall distribution (mean ± SEM, derived from the average of three technical replicates per study patient) of ddPCR derived: (**f**) IDH1.R132H mutant copies, (**g**) IDH1 wild-type copies, and (**h**) IDH1.R132H MAF % across the three IDH1.R132H mutant glioma subtypes. **f**–**h** Brown-Forsythe and Welch ANOVA test with multiple comparisons was performed to evaluate the statistical significance of observed differences: (**f**) Astrocytoma, Grade 2–3 vs Grade 4 (−264.9, *p* value 0.9371), Astrocytoma, Grade 2–3, vs Oligodendroglioma, Grade 2–3 (−1229, *p* value 0.0435), Astrocytoma, Grade 4 vs Oligodendroglioma, Grade 2–3 (−963.8, *p* value 0.3766) (**h**) Astrocytoma, Grade 2–3 vs Grade 4 (6.794, *p* value 0.6707), Astrocytoma, Grade 2–3, vs Oligodendroglioma, Grade 2–3 (−17.26, *p* value 0.0059), Astrocytoma, Grade 4 vs Oligodendroglioma, Grade 2–3 (−24.05, *p* value 0.0073). **i**, **j** Kaplan–Meier curves were evaluated among patients with IDH1 mutant glioma by stratifying the patient population using different parameters: (**i**) glioma subtype, and (**j**) IDH1.R132H tumor tissue MAF %, cut-off (≤38%, >38%). *P*-value was calculated using Log-Rank test. Source Data are provided as a Source Data file. Figure 2/panel A, B Created with BioRender.com released under a Creative Commons Attribution-NonCommercial-NoDerivs 4.0 International license (https://creativecommons.org/licenses/by-nc-nd/4.0/deed.en).

https://doi.org/10.1038/s41467-024-51332-7

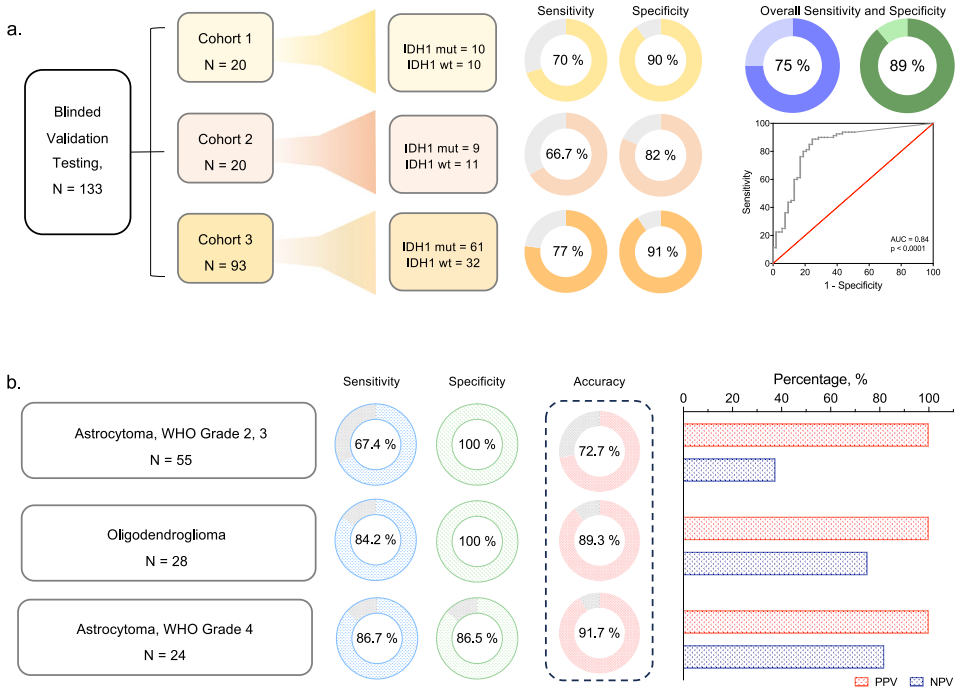

Fig. 3 | Clinical validation of the *mt*-IDH1$_{dx}$ assay and statistical evaluation of its diagnostic performance using plasma derived Extracellular Vesicle RNA. **a** Schematic summarizing the study population ($N = 133$) for blinded validation testing in three independent cohorts. Sensitivity and Specificity calculated for the individual cohorts and the combined study population. Area under curve (AUC) analysis performed to measure assay efficiency. This was done using Wilson/Brown method with results demonstrating an Area 0.8392 and standard error 0.03775 (95% CI: 0.7652–0.9131, p value < 0.0001). **b** A comparison of assay the sensitivity, specificity, and accuracy in the study population stratified by histological diagnosis (Astrocytoma, Grade 2–3, Oligodendroglioma, Grade 2–3, and Astrocytoma, Grade 4). Source Data are provided in Supplementary Tables 2, 3.

analysis based on disease parameters (Supplementary Fig. 5) was also performed.

Clinical validation of the *mt*-IDH1$_{dx}$ assay performance in EV RNA derived from patient plasma

mt-IDH1$_{dx}$ assay performance was evaluated in plasma samples across three blinded, validation cohorts ($N = 133$, Cohort 1; $n = 20$, Cohort 2; $n = 20$, Cohort 3; $n = 93$) (Fig. 3a) comprising histopathology confirmed IDH1mt glioma patients ($n = 80$), IDH1wt glioma patients ($n = 44$) and age-matched healthy controls ($n = 9$) (Fig. 3a). Two ml of plasma was processed from each sample (see Methods) and eight replicates analyzed at the final ddPCR step (Supplementary Tables 2, 3). The cut-off (i.e., number of positive replicates) for calling a sample positive was statistically determined by calculation of the Youden index (Supplementary Fig. 3d). Based on this calculation and clinical relevance, samples having at least three (≥3) positive replicates with IDH1.R132H MAF % greater than or equal to 0.06% based on Limit of Detection (LOD) experiment, were considered IDH1mt positive.

Baseline plasma testing results were as follows (Fig. 3a): Cohort 1; Sensitivity 70.0% (95% CI: 34.8–93.3%), Specificity 90.0% (95% CI: 55.5–99.8%), Cohort 2; Sensitivity 66.7% (95% CI: 29.9–92.5%), Specificity 81.8% (95% CI: 48.2–97.7%), Cohort 3; Sensitivity 77.1% (95% CI: 64.5–86.9%), Specificity 90.6% (95% CI: 75.0–98.0%) (Fig. 3a). Overall, across the study population ($N = 133$), our mt-IDH1$_{dx}$ assay detected IDH1.R132H mutation in plasma derived EV RNA with an overall sensitivity of 75.0% (95% CI: 64.1–84.0%), Specificity 88.7% (95% CI: 77.0–95.7%), and AUC 0.84 ($p < 0.0001$) (Fig. 3a). Positive predictive value (PPV) and negative predictive value (NPV) was determined to be 90.9% (95% CI: 82.3–95.6%) and 70.1% respectively (61.4–77.7%) (Fig. 3a). In a subset ($n = 9$) IDH1wt (by MGH clinical pathology) patient samples, IDH1mt signal was detected by plasma testing: Grade 4, Astrocytoma (Secondary GBM; $n = 3$), Primary GBM ($n = 4$), Multifocal GBM ($n = 1$) and low grade Glioneuronal tumor ($n = 1$). Subsequent *mt*-IDH1$_{dx}$ assay testing of tumor tissue (available in $n = 3$) derived RNA confirmed the presence of the IDH1mt signal. Of note, in the cases where plasma mt-IDH1$_{dx}$ testing was postive but clincial pathology reporting was negative, the pathology assessment of IDH1mt in the above cases (including $n = 3$ validated by *mt*-IDH1$_{dx}$ ddPCR testing) was clinically determined by Immunohistochemistry (IHC). Clinical information and demographics variables are summarized for IDH1mt (Supplementary Fig. 3e, Table 1) and IDH1wt (Supplementary Table 1) study population included in each individual cohort. Additional correlation analysis of EV RNA IDH1.R132H MAF % with various clinical and disease parameters was performed across different glioma subtypes (Supplementary Fig. 4).

In order to evaluate the blood-based *mt*-IDH1$_{dx}$ assay performance across different histological subtypes of IDH1mt gliomas, the study population was stratified into three groups (Fig. 3b): (i) Astrocytoma, Grade 2–3 ($N = 55$), (ii) Oligodendroglioma, Grade 2–3 ($N = 28$), and (iii) Astrocytoma, Grade 4 ($N = 24$). The assay was able to perform robust sensitive detection of common IDH1mt gliomas, i.e., low grade astrocytomas (67.4%, 95% CI: 52.0–80.5%) and oligodendrogliomas (84.2%, 95% CI: 60.4–96.6%) with a specificity of 100% (95% CI: 63.7–100%) (Fig. 3b). Furthermore, the *mt*-IDH1$_{dx}$ assay can also be used in conjunction with the radiological imaging as a companion diagnostic to accurately differentiate between the common IDH1mt glioma subtypes (Astrocytomas, grade 2–3: 72.7%, Oligodendroglioma, grade 2–3: 89.3%, Astrocytoma, grade 4: 73.0%). Finally, we also performed an experimental evaluation of rigor and reproducibility of the proposed *mt*-IDH1$_{dx}$ assay (Supplementary Fig. 2g).

Prognostication of the *mt*-IDH1$_{dx}$ assay across glioma subtypes

In addition to baseline clinical diagnostics, we also explored the viability of using blood-based detection of IDH1.R132H as a prognostication tool to predict survival outcomes. Cohorts described in Fig. 3 (Cohort 1, 2, 3) were combined here to perform prognostication

https://doi.org/10.1038/s41467-024-51332-7

Table 1 | IDH1.R132H mutant study population demographics and disease parameters

Parameter	Cohort 1, (*N* = 10) *n* (%)	Cohort 2, (*N* = 9) *n* (%)	Cohort 3, (*N* = 61) *n* (%)
Age (yr)			
≤40	5 (50.0)	1 (11.1)	30 (49.1)
>40	5 (50.0)	8 (88.9)	31 (50.8)
Gender			
Male	6 (60.0)	6 (66.7)	38 (62.3)
Female	4 (40.0)	3 (33.3)	23 (37.7)
WHO Grade			
2	5 (50.0)	2 (22.2)	17 (27.9)
3	5 (50.0)	6 (66.7)	31 (50.8)
4	0 (0.0)	1 (11.1)	13 (21.3)
Diagnosis			
Astrocytoma, Grade 2–3	9 (90.0)	6 (66.7)	32 (52.5)
Oligodendroglioma, Grade 2–3	1 (10.0)	2 (22.2)	16 (26.2)
Astrocytoma, Grade 4	0 (0.0)	1 (11.1)	13 (21.3)
Cortical Location			
Frontal	2 (20.0)	3 (33.3)	41 (67.2)
Parietal	2 (20.0)	2 (22.2)	4 (6.6)
Temporal	5 (50.0)	3 (33.3)	11 (18.0)
Other	1 (10.0)	1 (11.1)	5 (8.2)
Cerebral Hemisphere			
Dominant	6 (60.0)	5 (55.6)	34 (55.7)
Non-dominant	4 (40.0)	4 (44.4)	24 (39.3)
Tumor Volume (cm^3)			
<20	2 (20.0)	0 (0.0)	15 (24.6)
20–50	3 (30.0)	2 (22.2)	15 (24.6)
51–100	2 (20.0)	3 (33.3)	12 (19.7)
>100	2 (20.0)	3 (33.3)	13 (21.3)
ill-defined	1 (10.0)	1 (11.1)	5 (8.2)
Recurrence			
Yes	3 (30.0)	5 (55.6)	28 (45.9)
No	7 (70.0)	4 (44.4)	31 (50.1)
Post-Operative Treatment			
RT only	5 (50.0)	5 (55.6)	41 (67.2)
RT + TMZ	2 (20.0)	1 (11.1)	11 (18.0)
Clinical Trial Participant	3 (30.0)	1 (11.1)	4 (6.6)
Surveillance	1 (10.0)	3 (33.3)	9 (14.8)
MGMT status			
methylated	4 (40.0)	3 (33.3)	20 (32.8)
unmethylated	3 (30.0)	1 (11.1)	17 (28.9)
TP53 status			
wild-type	1 (10.0)	3 (33.3)	10 (16.4)
mutant	7 (70.0)	6 (66.7)	48 (78.7)
ATRX status			
wild-type	1 (10.0)	4 (44.4)	21 (34.4)
mutant	7 (70.0)	5 (55.6)	36 (59.0)
CDKN2A status			
wild-type	4 (40.0)	5 (55.6)	28 (45.9)
mutant	0 (0.0)	0 (0.0)	8 (13.1)

WHO World Health Organization, *RT* radiation therapy, *TMZ* Temozolamide, *MGMT* O^6-methyl-guanine-DNA methyl-transferase, *TP53* Tumor Protein 53, *ATRX* α-thalassemia/mental-retardation-syndrome-X-linked gene, *CDKN2A* cyclin-dependent kinase inhibitor 2A.

analysis. Patient population stratification via plasma-based EV RNA IDH1.R132H MAF, % (<0.15, ≥0.15) demonstrated an overall survival benefit in patients with higher (≥0.15%, 125.4 vs 87.2 months) mutational expression (Fig. 4a). The results indicating improved survival outcomes in lesions with higher MAF were in line with the previous observations made in the Kaplan–Meier analysis of tumor tissue cohort (Fig. 2j).

Next, EV RNA IDH1mt, IDH1wt copy numbers (Supplementary Fig. 3a–c), and overall IDH1.R132H MAF% distribution was compared across the three glioma subtypes (Fig. 4b). Interestingly, a similar pattern of IDH1mt enrichment was noted in the three histological variants in both tumor tissue (Fig. 2h) and plasma-derived EV mRNA (Fig. 4b). Oligodendroglioma subtype was associated with a 2-fold higher enrichment of IDH1mt EV RNA than astrocytoma, grade 2–3 (Oligodendroglioma: 1.28 ± 0.71, Astrocytoma, grade 2–3: 0.63 ± 0.32) and 3-fold higher enrichment than astrocytoma, grade 4 (0.38 ± 0.14) (Fig. 4b). An independent comparison of overall survival (OS) in the same groups demonstrated a significantly higher median OS (87.2–102.6 months) in subtypes expressing higher IDH1 MAF (low-grade astrocytoma, oligodendroglioma) versus the subtype with lower MAF (high-grade astrocytoma, 50.4 months) (Fig. 4c), again demonstrating a positive prognostic correlation between IDH1 MAF and overall survival (OS).

Finally, we determined the prognostication utility of EV RNA IDH1.R132H MAF, % in the glioma subtypes at cut-offs determined by population distribution in each group (Fig. 4d–f). In the low-grade astrocytoma group, no difference in short-term progression-free survival (PFS) was found between the two curves. However, there was a significant difference in long-term PFS (9.3 yr, 11 yr) with a longer median PFS seen in patients with higher (≥0.08%) EV RNA IDH1.R132H MAF determined at baseline diagnostics (Fig. 4d). Patient stratification via EV RNA IDH1.R132H MAF (<0.26%, ≥0.26%) in oligodendroglioma group demonstrated a much larger difference (208 vs. 74 months) in PFS with higher MAF (≥0.26%) conferring a better prognosis (Fig. 4e). The difference between the two survival curves was shown to be statistically significant at 6.2 yr and 7.3 yr follow-up timepoints (Fig. 4e). In the more aggressive subtype, i.e., grade 4 astrocytoma, a similar pattern was observed with higher MAF (≥0.12%) being a favorable prognostic factor (Fig. 4f). A higher baseline EV RNA IDH1.R132H MAF was associated with a 3-fold longer median PFS (91.4 vs. 50.4 months). Importantly, this glioma subtype has previously been reported to have poor survival outcomes versus low grade astrocytoma and oligodendroglioma. Interestingly, in our plasma-based prognostication analysis, the EV RNA IDH1.R132H MAF cut-off was an important tool in predicting short term PFS at 3.9 yr and 5.2 yr mark (versus longer follow-up timepoints in other subtypes), indicating the potential significance in a more rapidly progressing tumor lesion (Fig. 4f).

Overall, a higher plasma EV RNA IDH1.R132H MAF, % was identified as a favorable prognostic factor for predicting improved survival outcomes across all clonal subtypes. This is consistent with earlier findings of positive correlation between tumor tissue MAF and overall survival in an independent cohort.

Higher tumor analyte shedding rate in plasma correlates with improved overall survival

A subset of patients (tested in Fig. 3) was selected where matched tissue and plasma analysis was performed. The mt-$IDH1_{dx}$ assay was performed in matched tumor tissue and plasma samples ($n = 24$) across three IDH1mt glioma subtypes: Astrocytoma, grade 2–3 ($n = 14$), Oligodendroglioma, grade 2–3 ($n = 5$), and Astrocytoma, grade 4 ($n = 5$). Statistical evaluation of the differential expression of IDH1mt (Fig. 5a) and IDH1wt (Fig. 5b) in tumor tissue versus. plasma was performed via plotting log fold-change (FC, Log_2 ratio = Avg. Mut/WT, Plasma/Avg. Mut/WT, Tissue) (*y*-axis) against average expression

https://doi.org/10.1038/s41467-024-51332-7

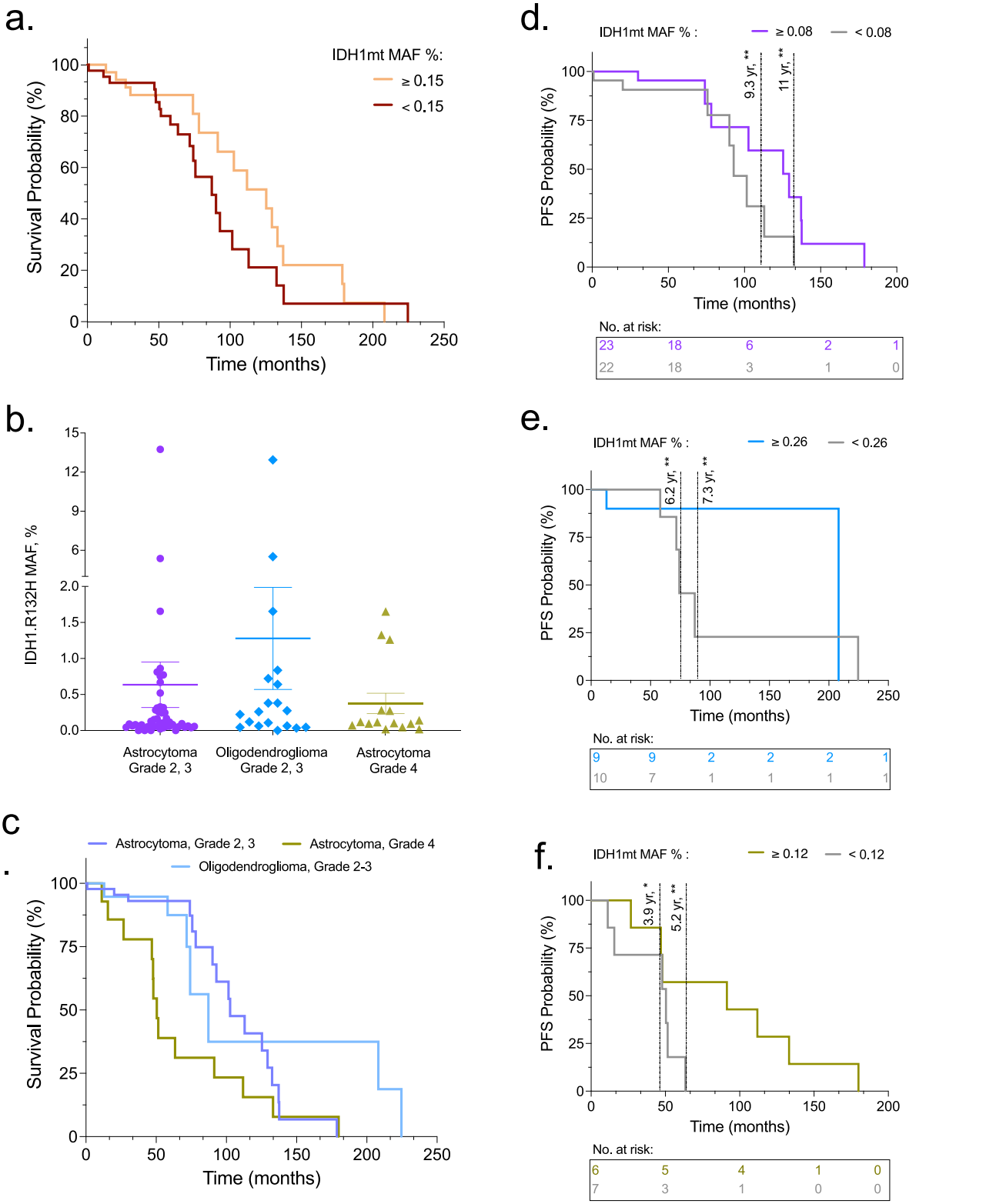

Fig. 4 | Assessment of the prognostic significance of blood-based detection of IDH1.R132H across glioma subtypes using the *mt*-IDH1$_{dx}$ assay. a Kaplan–Meier analysis performed among IDH1 mutant patients using EV RNA IDH1.R132H MAF % cut-off determined by plasma testing. **b** Scatter-dot plot (each data point represents an individual patient; mean of eight technical replicates) demonstrating the overall distribution (mean ± SEM, denoted by horizontal line and error bars) of EV RNA IDH1.R132H MAF % across the three IDH1.R132H mutant glioma subtypes: Astrocytoma, Grade 2, 3 ($n = 46$, biological replicates), Oligodendroglioma, Grade 2, 3 ($n = 19$, biological replicates) and Astrocytoma, Grade 4 ($n = 15$, biological replicates). **c**–**f** Kaplan–Meier curves were evaluated among patients with IDH1 mutant glioma using different approaches: (**c**) patient stratification by histological diagnosis, (**d**–**f**) EV RNA IDH1.R132H MAF% cut-off unique to each subtype (**d**; Grade 2, Astrocytoma, **e**; Grade 2–3, Oligodendroglioma, **f**; Grade 4, Astrocytoma). *P*-value was calculated using Log-Rank test. Source Data are provided as a Source Data file.

https://doi.org/10.1038/s41467-024-51332-7

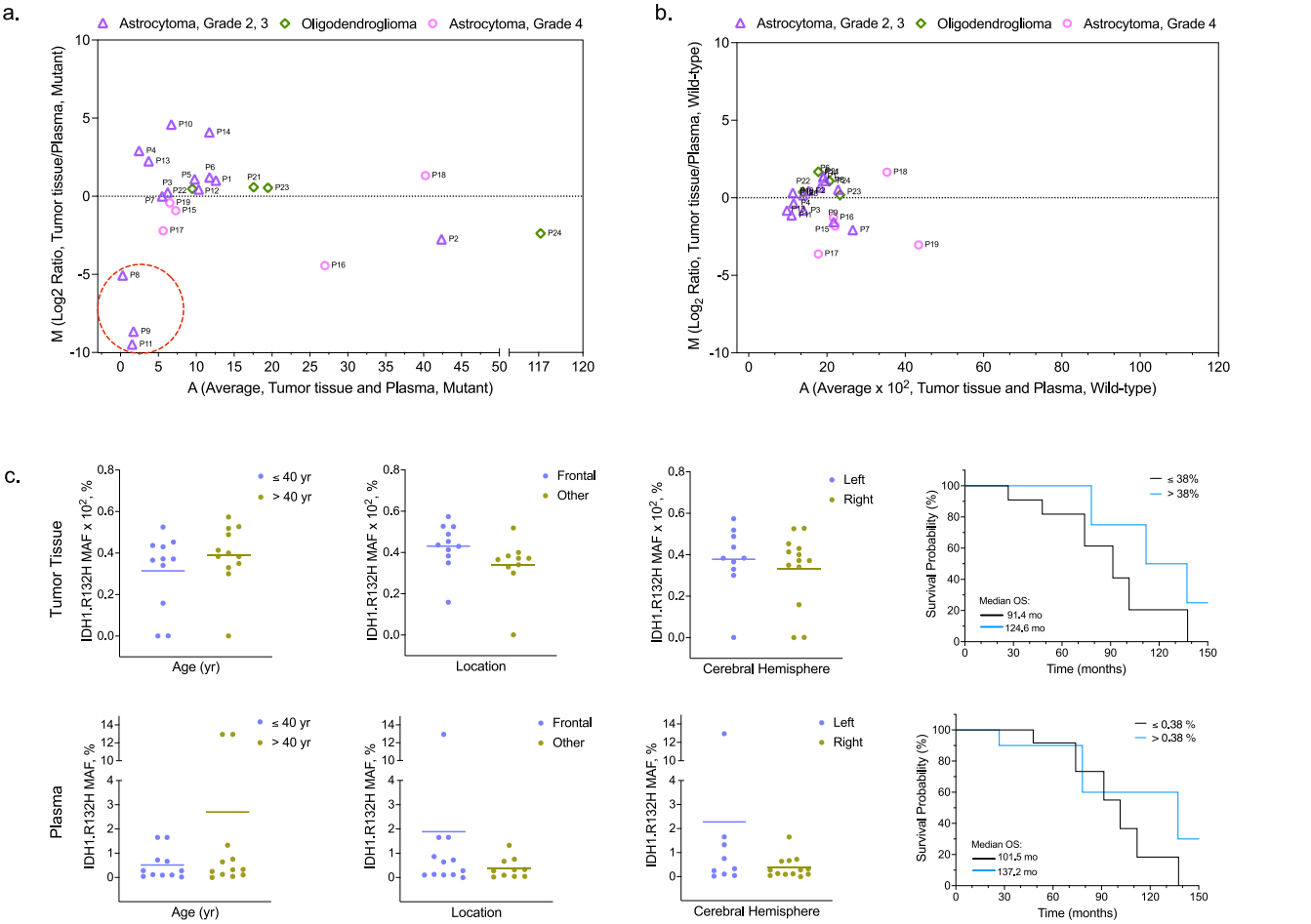

Fig. 5 | The shedding rate of IDH1.R132H mutant tumors varies among the different subtypes of gliomas. a, **b** MA plots comparing the differential enrichment of (**a**) IDH1.R132H (Mut) expression and (**b**) IDH1 wild-type (Wt) expression in matched ($n = 24$) tumor tissue derived total RNA versus plasma-derived EV RNA. MA plots were created by plotting M value (*y*-axis; Log_2 ratio = Avg. Mut/WT, Plasma/Avg. Mut/WT, Tissue) against A value (*x*-axis; Average, Mut/Wt tissue and Mut/Wt plasma). **a** Patients encircled (red circle demonstrated the highest enrichment in plasma. **c** Scatter-dot plots demonstrating the overall IDH1.R132H MAF% distribution in matched ($n = 24$) tumor tissue (top) and plasma samples (bottom) across multiple variables (Age, Cortical location, Cerebral hemisphere). Kaplan–Meier survival analysis using IDH1.R132H MAF % cut-off as a prognostic indicator in tumor tissue (**c**: top, right) and plasma (**c**: bottom, right). Source Data are provided as a Source Data file.

(x-axis; Average, Mut/Wt tissue and Mut/Wt plasma) of mutant (Fig. 5a) and wild-type (Fig. 5b) targets. We observed considerable variation in tissue versus plasma enrichment of IDH1mt RNA across the three clonal subtypes (Fig. 5a). In contrast, IDH1 wild-type RNA showed similar expression levels in tumor tissue-derived RNA and plasma-derived EV RNA across the low-grade and high-grade gliomas (Fig. 5b).

Among patient samples with higher enrichment of the IDH1mt signal in plasma, Grade 3 Astrocytomas ($n = 4$, P2, P8-9, P11) were shown to demonstrate the highest shedding rate than other subtypes (Fig. 5a, encircled in red). Comparing all subtypes, low grade astrocytomas were associated with a 3-fold higher enrichment (Log_2 FC: 6.5 ± 3.1) of IDH1mt signal in EV RNA versus the more aggressive grade 4 subtype (Log_2 FC: 2.0 ± 1.8) (Fig. 5a). Importantly, tumor lesions demonstrating higher shedding rate as statistically determined by M value (enrichment in plasma) were also associated with an improved overall survival (OS). In this case, the difference in median OS between low vs. high grade astrocytomas was statistically significant ($p = 0.038$, *) with a 2-fold longer OS in higher shedding grade 2–3, astrocytoma (129.5 months) than the lower shedding grade 4, astrocytoma lesions (65.6 months).

Tumor tissue enrichment was noted for ($n = 9$) Astrocytomas with an average M value of 1.98 (0.25–4.59) (Fig. 5a). To compare the clinical outcomes and prognosis of astrocytomas with higher versus lower shedding rates, Kaplan–Meier analysis was performed. A statistically significant difference ($p = 0.03$, *) was found between the two survival curves. Astrocytomas demonstrating higher shedding of EV mRNA ($n = 5$) were associated with a longer median OS (129.5 months) than the lesions less likely to shed ($n = 9$, 72.2 months).

Next, based on previous observations of IDH1.R132H MAF distribution among different patient characteristics (independent tissue and plasma analysis), we proceeded to test this in the matched tumor tissue (Fig. 5c, top) and plasma samples (Fig. 5c, bottom). Overall, similar trends were seen in both analyses (Fig. 5c), with higher IDH1.R132H MAF (tissue and EV RNA) reported in: i) age group >40 yr, ii) tumors in frontal lobe, and iii) lesions in dominant (left) hemisphere. Finally, consistent with previous findings, IDH1.R132H MAF served as a positive prognostic factor in tumor tissue and plasma, with higher baseline MAF (tissue: >38%, plasma: >0.38%) associated with a longer median OS (Fig. 5c).

Longitudinal glioma monitoring using the *mt*-$IDH1_{dx}$ assay, correlates with radiological and clinical outcomes

In the final phase of clinical validation, we tested the utility of *mt*-$IDH1_{dx}$ in longitudinal disease monitoring and surveillance. A cohort of $n = 8$ plasma samples (subset of the patients tested in Fig. 3) was included with evaluation at multiple clinical timepoints: tumor

https://doi.org/10.1038/s41467-024-51332-7

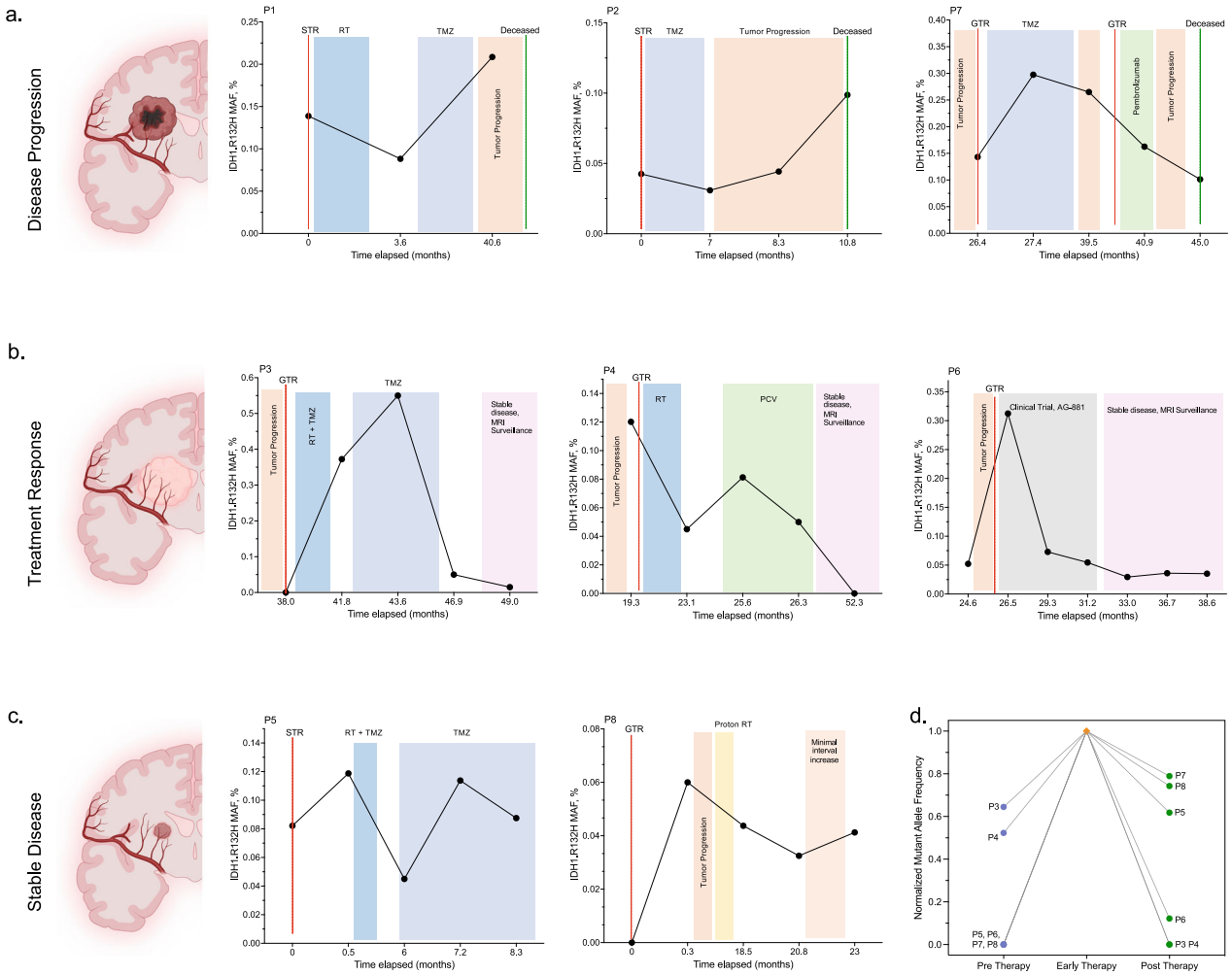

Fig. 6 | Assessing monitoring and surveillance of IDH1.R132H mutant gliomas during the course of clinical therapy. a–c Testing of the optimized ddPCR assay in plasma samples (2 ml) collected longitudinally in a cohort of $n = 8$ (labeled, P1-P8) patients. Individual graphs summarizing the EV RNA IDH1.R132H, MAF % (*y*-axis, mean of 8 replicates) at each clinical time-point (*x*-axis, time elapsed from baseline detection) with the affiliated radiological findings and clinical outcomes. Study population divided into three groups based on clinical outcomes: (**a**) disease progression, (**b**) treatment response, and (**c**) stable disease. **d** Line plot (third panel, bottom-right) demonstrating the overall trend in measured EV RNA IDH1.R132H MAF % (normalized, described in methods) levels at selected clinical timepoints of treatment: pre-, early- and post- therapy. GTR: Gross total resection, STR: Sub-total resection, Proton RT: Proton therapy, TMZ: Temozolamide, RT: Radiation therapy, PCV: Procarbazine, Lomustine, and Vincristine. Source Data are provided as a Source Data file. Figure 6/A-C Created with BioRender.com released under a Creative Commons Attribution-NonCommercial-NoDerivs 4.0 International license (https://creativecommons.org/licenses/by-nc-nd/4.0/deed.en).

progression, pre-, early-, and post- therapy, MRI surveillance, and stable disease (Fig. 6). The study population ($n = 8$) was divided into three groups based on different disease outcomes: i) Disease Progression (P1, P2, P7, Fig. 6a), ii) Treatment Response (P3, P4, P6, Fig. 6b), and iii) Stable (or Minimal Residual) Disease (P5, P8, Fig. 6c).

In the disease progression group (P1, P2, P7, Fig. 6a), different glioma subtypes were represented: P1 (Astrocytoma, Grade 2), P2 (Astrocytoma, Grade 3), P7 (Astrocytoma, Grade 4). Across all time points, P1 showed rising plasma levels of IDH1.R132H MAF, consistent with disease progression as evidenced by surveillance MRI and neurological deterioration. Radiological imaging performed shortly before the second plasma sampling, was inconclusive for pseudo- versus true tumor progression. However, subsequent tumor tissue testing (stereotactic biopsy) confirmed progression to grade 4 lesion, and this was consistent with the blood-based findings. Similarly, in both P2 and P7, the plasma based EV RNA IDH1.R132H MAF remained high and was consistent with progressive disease (according to MRI findings), correlating with worsening clinical outcomes.

In the treatment response group (P3, P4, P6, Fig. 6b), across all three patients, we observed a steep decline in blood-based IDH1.R132H MAF, with plasma levels dropping to undetectable levels in 2/3 at the last follow-up time-point available to us. This was in perfect concordance with the radiological imaging findings indicating stable disease and good treatment response. Interestingly, in all three patients we observed an early spike in the IDH1mt plasma-levels following treatment initiation (P3: TMZ, P4: PCV, P6: AG-881) followed by progressively declining IDH1mt signal over the course of treatment. In P6, the short-term follow-up plasma testing demonstrated a very low, but persistent IDH1mt signal. Importantly, this correlated with the MRI findings of unchanged T2/FLAIR abnormality which remains under surveillance and has not progressed (based on last clinical follow-up).

In the stable disease group (P5, P8, Fig. 6c), we observed similar concordance of plasma testing and clinical evaluation with P5 and P8 presenting with an overall stable disease. Surveillance MRI performed during the treatment course of P5 was inconclusive at first for pseudo progression versus treatment related effects. However, pseudo progression was later confirmed based on a decrease in contrast enhancement and T2/FLAIR hyperintensity. These findings were concordant with the drop in IDH1mt signal measured in plasma testing. P8 also had an initial increase in IDH1.R132H MAF corresponding to tumor

progression on MRI. Follow-up plasma testing correlated with treatment response and stable disease on surveillance imaging.

Interestingly, a consistent increase in the plasma IDH1mt levels was observed in response to various treatment modalities. This is summarized (Fig. 6d) for multiple patients by performing normalization of EV RNA IDH1.R132H MAF (see Methods) and comparing the signal at three time-points: pre-, early-, and post-therapy. This potentially highlights an important biological process of tumor shedding and release of tumor derived EVs into systemic circulation, following treatment initiation.

Discussion

Historically, glioma classification relied largely on histology and immunohistochemistry[17]. Integration of molecular alterations, specifically IDH1.R132H, was first introduced in 2016[18] WHO Classification of CNS tumors and later expanded in 2021[19] after its breakthrough discovery in gliomas in 2008[2]. Accurate diagnosis of this unique molecular variant is critical in determining the clinical and surgical management of an expansive lesion on magnetic resonance image (MRI). Typically, hyperintensity on T2-weighted images and T2-fluid-attenuated inversion recovery sequences (FLAIR) features are highly suggestive of a likely IDH1.R132H mutant glioma[20,21]. However, definitive diagnosis still requires the histopathology assessment of tumor tissue. Here, we present a blood-based ddPCR assay that can detect IDH1.R132H mutation in plasma derived EV mRNA with an overall sensitivity of 75.0% (95% CI: 64.1–84.0%), Specificity 88.7% (95% CI: 77.0–95.7%), and AUC 0.84 ($p < 0.0001$). In addition to baseline diagnosis, we also report correlation between IDH1.R132H MAF (tumor tissue, plasma) and key clinical variables: (i) overall survival, (ii) tumor shedding rate, (ii) treatment outcomes. Overall, the proposed *mt*-$IDH1_{dx}$ assay can be utilized for blood-based diagnosis, prognostication, and longitudinal monitoring.

Previous work in liquid biopsy (plasma, CSF) based assessment of IDH1.R132H mutational status has predominantly utilized cell free DNA (cfDNA)[22–26] as the candidate biomarker with an overall limited sensitivity (25–63%)[22–26]. Results from our testing show that an RNA based assay is more sensitive than DNA across focal and spatial tumor tissue analysis of different IDH1 mutant glioma subtypes. Interestingly, oligodendrogliomas ($n = 7$) and grade 4 astrocytomas ($n = 4$) showed a wider distribution of the IDH1 mutant and wild-type RNA:DNA ratios, with astrocytomas, grade 2–3 ($n = 12$) showing a more homogeneous distribution (Figs. 1b, c, 2f, g). This is likely a reflection of differences in tumor biology, including the extent of tumor infiltration[27], as well as a wider age range distribution in oligonderogliomas than astrocytomas as previously reported[28]. Importantly, in our cohort, astrocytomas also had a lower age range (44.0) and coefficient of variation (22.6%) compared to oligodendrogliomas (age range: 53, coefficient of variation: 30.7%).

mt-$IDH1_{dx}$ assay performance was evaluated in comparison to the traditional gold standard clinical pathology testing. Overall, in our study we had $n = 2$ tissue and $n = 3$ plasma samples that were in discordance with histopathology assessment. Notably, using our *mt*-$IDH1_{dx}$ assay we identified the IDH1.R132H mutation in a subset of astrocytoma patients originally classified as IDH1.R132H wild-type ($n = 2$; expressing IDH1.R132C or IDH1.R132S) based on pathology testing. This discordance can be attributed to several factors: (i) difference in sensitivity between ddPCR and IHC methods, (ii) preferential use of cost-effective (but, less sensitive) testing techniques (IHC, DNA qPCR) in patients ≥55 years of age with radiological suspicion of grade 4 astrocytoma (previously classified as Glioblastoma) due to low pre-testing probability of the presence of IDH1 mutation[29], (iii) tissue sampling errors (insufficient, non-viable), and (iv) intratumoral spatial heterogeneity. The presence of multiple, genetically distinct subclones with diverse evolutionary potential has been well described for IDH1 wild-type GBM[30,31] and more recently, IDH1.R132H mutant glioma[32–34]. Astrocytomas (grade 3–4) harboring such "subclonal IDH1 mutation" (defined as tumor cell fraction with IDH mutation ≤0.67) have also been reported[35]. Hence, sensitive plasma testing can facilitate a more comprehensive determination of mutational status as shown by the confirmation of the IDH1mt signal in tumor tissue (following positive signal in plasma). Considering the challenges encountered in standard clinical testing, our tissue and blood-based *mt*-$IDH1_{dx}$ assay emerges as a promising, feasible platform for rapid and sensitive diagnostics, overcoming the limitations posed by disease heterogeneity and technical limitations.

Here we also analyzed the correlation between IDH1.R132H MAF (tumor tissue, plasma) and multiple disease parameters. Notably, we found consistently similar trends in independent tumor tissue (Fig. 2) and plasma (Fig. 4) cohorts. Most striking observation was that high tissue and plasma IDH1.R132H MAF served as a positive prognostic factor, associated with longer OS across all subtypes. While it is well established that oligodendroglioma is associated with improved overall survival[36], herein we report that the improved OS is shown to correlate with increased plasma MAF and tumor tissue MAF. Furthermore, IDH1.R132H MAF distribution in matched and unmatched plasma/tissue samples highlighted key trends, with higher MAF seen in the following variables: frontal location, left hemisphere, and age ≳40 yr. Finally, tissue/plasma copy enrichment analysis indicated variation in glioma solid tumor shedding rate across different subtypes. While the measured IDH1wt expression was consistent in both tissue (total RNA) and plasma (EV RNA), IDH1mt expression showed considerable variation, highlighting further the significance of investigating heterogeneity of IDH1.R132H mutant tumor biology, specifically in astrocytomas and oligodendrogliomas. Additionally, tumor lesions with higher shedding levels (low-grade astrocytomas) were associated with overall improved survival as compared to lower shedding tumors (high-grade astrocytomas; Fig. 5). A similar trend has been observed for other cancers like hepatocellular carcinoma[37], melanoma[38], pancreatic and colon cancer[39], and in vivo glioma models[40].

Lastly, the *mt*-$IDH1_{dx}$ blood-based assay was analyzed in longitudinal settings to determine its utility in disease monitoring, predicting treatment response, and surveillance. Overall, results demonstrated concordance with the radiological imaging findings and/or tissue biopsy assessment across different clinical outcomes: tumor progression, treatment response, stable disease. Interestingly, in two patients (P3, P8) the assay was not able to detect the mutation at baseline testing. P3 had an initial diagnosis of Astrocytoma, Grade 2 with tumor volume below $1cm^3$. Based on our correlation analysis (Fig. 5), IDH1.R132H MAF tends to be lower in non-frontal, right-sided lesions, which is where this patient's was located. Furthermore, the lesion measured 13 × 23 mm in maximum axial dimension. Interestingly, as per clinical pathology tissue assessment, the lesion was IDH1 wild-type by IHC but later confirmed IDH1mt by Snapshot analysis. However, following tumor progression the assay detected IDH1mt in plasma with levels showing correlation to the disease course. A second patient (P8) demonstrated a similar trend where the IDH1mt signal was not detected at the first time point (pre-surgery) but was detected at high levels at a later time-point. Similarly, P8 had a low disease burden at initial diagnosis but progressed following initial surgical resection as shown by an enhancing radiological signal and worsening cognitive function. Another key experimental observation was the overall trend in measured EV RNA IDH1.R132H MAF (normalized) across different patients receiving TMZ and PCV (Fig. 6d). The initial rise followed by decline in levels provides insight into the tumor shedding mechanism in response to treatment and hence, interpretation of increased tumor derived analytes in the bloodstream. It has been shown that EVs secreted by melanoma cells in response to chemotherapy modulate and predict the tumor response to alkylating drugs[38]. However, this has not been investigated in the realm of gliomas. We hypothesize that EV RNA cargo can be serially quantified to not only determine but also

predict treatment response. For instance, in our analysis patients with complete treatment response (radiological evidence; P3, P4, P6) had a much larger decline in MAF following initial rise as compared to patients with radiological evidence of residual disease (P5, P7, P8). Interestingly, while the MAF does correlate with overall outcomes in treatment naive glioma patients, the pattern is different in recurrent tumors undergoing treatment[41,42]. These differences are likely a reflection of the evolution in tumor biology, mutational landscape, tumor microenvironment, and blood-brain-barrier disruptions[41,42]. Important to consider is also the time period (often up to years) between initial diagnosis and recurrence. Importantly, this current data on IDH1.R132H as well as our previous work on TERTp[13] and EGFRvIII[14], consistently show a higher MAF and/or copy number at final tumor recurrence time point as compared to baseline. The glioma treatment likely alters the shedding rate in the plasma of glioma patients, shifting its association from overall survival to the treatment course of the disease. Recent work by our team also highlights a spike in the shed analyte into biofluids (CSF and plasma) at the early therapy timepoint and underscores the value of monitoring treatment course using liquid biopsy especially in targeted therapeutics, including CAR T Cell treatment[43].

In summary, the field of liquid biopsy diagnostics and theranostics is evolving rapidly. Gliomas, a diverse group of tumors in the central nervous system, exhibit a wide range of molecular and epigenetic characteristics. The IDH1.R132H mutation, present in both low-grade and high-grade gliomas, stands out as a distinct alteration with significant prognostic implications. We introduce a highly sensitive platform designed for rapid testing, offering multiple clinical applications, including (i) diagnosis, (ii) prognostication, (iii) monitoring of treatment response, and iv) longitudinal disease monitoring and surveillance. Future efforts will be directed towards conducting extensive testing in larger and more varied patient populations to decipher the assay performance in different clinical settings. This step is crucial for achieving a better understanding of tumor biology and addressing the challenges of integrating liquid biopsy into clinical practice.

Methods

Our study was conducted in accordance with principles for human experimentation as defined in the U.S. Common Rule and was approved by the Human Investigational Review Board of each study center under Partners institutional review board (IRB)-approved protocol number 2017P001581. Samples were collected from patient population undergoing treatment at Massachusetts General Hospital.

Study population

Disease group participants recruited from the clinics to our biobank are not compensated for participation. Healthy control participants recruited from the general public are offered a monetary compensation for each blood draw they complete. The study population ($N = 133$) consisted of IDH1.R132H mutant; $n = 80$, IDH1 wild-type; $n = 44$ and age matched healthy controls; $n = 9$). Brain tumor patients aged 18 years or older underwent surgery at the Massachusetts General Hospital (MGH) for biopsy or resection of a primary tumor lesion. Gender and/or sex was not considered in the study design. The gender and/or sex of all participants was determined based on self-report. Clinical IDH.R132H status was established with either immunohistochemistry (IHC), Rapid IDH1 Analysis (DNA-based qPCR), or by the MGH SNaPShot Panel. Additional inclusion criteria for the study population included histopathological confirmation of disease. Healthy control participants with a history of oncologic, neurologic, or ongoing infectious conditions were excluded from the study. The study was performed on samples collected between 2014 and 2024. All IDH1.R132H samples were included from the biobank and matched with IDH-wild-type controls. Patient demographics and clinical parameters are depicted in an Oncoprint format in Supplementary Fig. 3e and in table format in Table 1 and Supplementary Table 1.

Tumor tissue processing

Tumor tissue was micro-dissected and suspended in RNAlater (Ambion) or flash-frozen and stored at −80 °C.

Patient plasma processing

Whole blood was collected using K2 EDTA tubes with an inert gel barrier (BD Vacutainer Blood Collection Tubes), from pre-operatively placed arterial lines or venipuncture. Within 2 h of collection, samples were centrifuged at 1100 x g for 10 minutes at 20 °C to separate the plasma from the hematocrit and filtered using 0.8 μM filters. 1 ml aliquots were stored at −80 °C for later downstream analysis. With the exception of the longitudinal samples, all baseline samples were collected prior to surgical resection.

RNA and DNA Isolation from tumor tissue

Frozen tumor tissue was thawed and lysed in 1–2 ml of ice-cold Trizol Reagent (ThermoFisher). Lysate was homogenized by passing through a 20-gauge RNAse-free needle 10 times. Total RNA was then extracted as per the manufacturer's protocol and eluted in 20 μl of nuclease-free water (Invitrogen). All RNA samples (cell lines, tumor tissue) were assessed for purity with the NanoDrop One spectrophotometer (ThermoFisher, Waltham, MA, USA,). Agilent RNA 6000 pico kit was used with Agilent Technologies 2100 Bioanalyzer (Waldbronn, Germany) to determine the concentration and RIN (RNA Integrity Number) value of the samples. Isolated RNA was stored at −80 °C prior to downstream analysis.

Co-isolation of DNA and RNA from tumor tissue

Frozen tumor tissue was thawed on ice. For each sample, DNA and RNA extraction was done in parallel using AllPrep DNA/RNA/miRNA Universal Kit (QIAgen), per the manufacturer's recommendations. DNA was eluted in 100 μl of the elution buffer (QIAgen) and stored at −20 °C until further processing. RNA was eluted in 20 μl of nuclease-free water (QIAgen) and stored at −80 °C until further processing.

EV RNA extraction from plasma samples

In order to isolate the analyte of interest, 2 ml plasma was obtained from each clinical sample (IDH.R132H mut, IDH wild-type, Healthy) and thawed on ice. Extracellular vesicle RNA (EV RNA) was isolated using the ExoLution™ kit, per the manufacturer's recommendations. EV RNA was eluted in 17 μl of nuclease-free water (Qiagen) and assessed for concentration and purity with the NanoDrop One spectrophotometer (ThermoFisher Scientific).

Co-isolation of EV RNA, EV DNA, and cfDNA from plasma samples

In order to isolate the analyte of interest, 2 ml plasma was obtained from each clinical sample (IDH.R132H mut, IDH wild-type, Healthy) and thawed on ice. ExoLutionPlus™ kit was utilized for one step isolation of EV RNA, EV DNA, and cell free DNA (cfDNA). Isolated multianalyte was eluted in 17 μl of nuclease free water (Qiagen) and assessed for concentration and purity with the NanoDrop One spectrophotometer (ThermoFisher Scientific).

Reverse transcription

Messenger RNA (mRNA) isolated from tumor tissue and cell lines, and EV RNA isolated from plasma samples, was reverse transcribed into cDNA using the SuperScript™ VILO™ cDNA Synthesis Kit (ThermoFisher Scientific). The protocol was performed as per the manufacturer's instructions. Briefly, the 20 μl reaction volume was prepared using 4 μl of 5X VILO™ Reaction Mix, 2 μl of 10X SuperScript™ Enzyme Mix, RNA (tumor tissue: 1 μl, Plasma (EV RNA): 16 μl), and DEPC-treated

water. The thermocycling conditions were as follows: 25 °C for 10 min, 42 °C for 60 min, and termination at 85 °C for 5 min. The resulting cDNA was used immediately or stored in −20 °C for later use.

Primers and probes

Through the course of optimization and preliminary testing, at least six different primer pairs specific to IDH.R132H were designed and tested. The primer sets generated amplicons of varying lengths, ranging from 49 bp to 89 bp. The key criteria in selecting the optimal primer set included; target amplicon size <100 bp, minimum formation of primer dimers, and absence of non-specific products. Tools used to design and assess different parameters include Primer-BLAST, Serial Cloner and Primer3Plus. Different primer sets were also compared on the basis of GC content, T_m (°C) mismatch, self-dimerization and hairpin formation. The final primer set selected for further optimization produced a target amplicon of 62 bp. Sequence for primers and probe are as follows: Forward mRNA primer (5′-AGTGGATGGGTAAAACC-3′), Reverse mRNA primer (5′-GATCAATACAGAGCAAC-3′, 3′-GTTGCTCT GTATTGATC-5′, IDH Mutant mutant probe (5′-/FAM/TCATAG + GTC + ATC + ATG + CTTA/IABkFQ/−3′), and IDH Wild-type probe (5′-/HEX/ TCATAG + GTC + GTC + ATG + CTTA/IABkFQ/−3′). All oligonucleotide preparations were synthesized by ThermoFisher Scientific and Integrated DNA Technologies. Primers were purified by desalting and resuspended in DEPC-treated water, at a final concentration of 100 µM. Mutant and Wild-type probes were HPLC purified and resuspended in 1xTE 100 pmol/µl.

Wild-type blocker

To facilitate minimization of wild-type signal amplification (or increase signal to noise ratio) during preamplification step, three different wild-type blockers were designed and tested. All oligonucleotide preparations were synthesized by Integrated DNA Technologies and resuspended in DEPC-treated water, at a final concentration of 100 µM. The wild-type blockers were designed with selected 5′ modification and the sequences are as follows: Wt1 (5′-CATAGGTCTCATGCTTA/3Phos/−3′), Wt2 (5′-CCCCATAAGCATGAGACCTATG /3Phos/−3′), Wt3 (5′-CCCCA-TAAGCATGACGACCTATG /3Phos/−3′). As per initial testing, Wt1 and Wt3 blockers were selected for further testing (Supplementary Fig. 2f. Following optimization in tumor tissue and plasma, Wt3 sequence was selected as the wild-type blocker.

Optimized droplet digital PCR (ddPCR) assay in tumor tissue and cell lines

Droplet digital PCR (ddPCR) was performed using purified cDNA obtained from reverse transcription of RNA isolated from cell lines and tumor tissue. The ddPCR reaction was performed in the Applied Biosystems™ 96-well Thermal Cycler (ThermoFisher Scientific) in a final volume of 20 µl. The optimized reaction mixture was prepared using 10 µl of ddPCR Supermix for Probes (no dUTP) (Bio-Rad), 1000 nM forward and reverse primers and 250 nM mutant and wild-type probe, cDNA, and water. The prepared reaction mixture was transferred to the wells of DG8 cartridge. To generate the droplets, 65 µl of Droplet generation oil for probes (Bio-Rad) was added and the plate was loaded into the QX200 Droplet generator (BioRad). The droplet emulsions were then carefully transferred to a semi-skirted, PCR-clean 96 well plate (Eppendorf) using a multichannel pipette. Lastly, the plate was sealed using PX1 PCR plate sealer (Bio-Rad). Based on the annealing temperature gradient optimization experiment, the final thermal cycling conditions were as follows: initial enzyme activation at 95 °C (51% ramp) for 10 min, then 40 cycles of denaturation at 94 °C (51% ramp) for 30 s, and annealing/extension at 51.0 °C for 1 min, followed by enzyme inactivation at 98 °C for 10 min and final hold at 4 °C until analysis. Droplets were analyzed using QX 200 droplet reader (Bio-Rad) and data were acquired and analyzed with QuantaSoft analysis software (Bio-Rad).

Optimized droplet digital PCR (ddPCR) assay in plasma derived extracellular vesicles (EVs)

Droplet digital PCR (ddPCR) was performed using purified cDNA obtained from reverse transcription of EV RNA isolated from plasma samples. For plasma samples, detection of low levels of mutant EV RNA was enhanced via PCR pre-amplification. The pre-amplification ddPCR was performed in the Applied Biosystems™ 96-well Thermal Cycler (ThermoFisher Scientific) in a final volume of 20 µl. The optimized reaction mixture was prepared using 6.5 µl of cDNA, 10 µl of SsoAdvanced™ PreAmp Supermix (Bio-Rad), 100 nM forward and reverse primers, 200 nM wild-type blocker, and water. Each plasma sample cDNA was preamplified in triplicates (three preamp well, 20 µl reactions). The thermocycling conditions were as follows: initial enzyme activation at 95 °C (51% ramp) for 10 min, then 10 cycles of denaturation at 94 °C (51% ramp) for 30 s, and annealing/extension at 51.0 °C for 1 min, followed by enzyme inactivation at 98 °C for 10 min. Following preamplification, the replicates from each plasma sample were pooled. Preamplified product was then diluted by adding 31 µl of water to 1 µl preamplified product. The final ddPCR was performed using the diluted pre-amplified product in a final reaction volume of 20 µl. The reaction mixture was prepared using 2 µl of diluted pre-amplified product, 10 µl of ddPCR Supermix for Probes (no dUTP) (Bio-Rad), 1000 nM forward and reverse primers and 250 nM mutant and wild-type probe. Each individual sample was run in eight replicates. The final thermal cycling conditions were as follows: initial enzyme activation at 95 °C (51% ramp) for 10 min, then 40 cycles of denaturation at 94 °C (51% ramp) for 30 s, and annealing/extension at 51.0 °C for 1 min, followed by enzyme inactivation at 98 °C for 10 min and final hold at 4 °C until analysis. Droplets were analyzed using QX 200 droplet reader (Bio-Rad) and data were acquired and analyzed with QuantaSoft analysis software (Bio-Rad).

Droplet digital PCR (ddPCR) dMIQE 2020 guideline compliance

This section of the methods describes our compliance with the updated 2020 dMIQE Guidelines for the technical development of a plasma-based ddPCR assay for the IDH.R132H mutation detection. Specimen type numbers, sampling procedure, aliquotation, conditions and duration are provided in the following sections of the Methods: Study Population, Tumor Tissue Processing, Cell Lines, and Plasma Processing. Details about the specific Extraction techniques, Nucleic Acid Assessment/Storage, and Reverse Transcription are provided in sections: RNA Isolation from cell lines and tumor tissue, and Exosomal RNA Isolation from plasma samples. Information about the ddPCR Oligonucleotides and its target sequences are provided along with the protocol both in Supplementary Fig. 1 and in the section entitled Primers and Probe. Details about the assay analytical validation are provided in Fig. 1. Finally, information regarding data analysis is provided both in the Results and Methods (see below).

Quantification of IDH.R132H mutation in plasma

The number of IDH1.R132H copies per mL of plasma was calculated from QuantaSoft data as follows: Copies/ml plasma = C EV/TV/P where C = copies per 20 µL, EV = exNA elution volume (µl), TV = exNA input into ddPCR reaction (µl) and p = plasma volume (ml). Only samples with >10,000 droplets/well were included in the analysis. Eight wells are analyzed in parallel for each sample. A positive sample is considered when at least three out of eight replicates have a signal. A number of IDH1 wild-type copies per ml of plasma was calculated using the same formula. We report IDH1.R132H Mutant Allele Frequency (MAF, %) calculated as follows: IDH1.R132H copies/ (IDH1.R132H copies + IDH1 wild-type copies) x 100%.

Statistical analysis

Statistical analysis was performed using the two-tailed Student's *t*-test (2 groups) and Ordinary one-way ANOVA (Analysis of Variance, >2

groups) in GraphPad Prism Version 10.1.1 software and $p < 0.05$ was considered to be statistically significant. The results are presented as Mean ± SEM. For normalization of longitudinal monitoring data (Fig. 6d), the statistical normalization was performed using GraphPad Prism. Briefly, it normalizes data between 0 and 100%, where zero is defined as the smallest value (MAF %) in each data set and one hundred is defined as the largest mean (MAF %). Data from each patient are normalized to a value in (0,1) so that the minimum within the patient takes value 0, the maximum takes value 1, and the value in between is normalized to the proportion between the minimum and the maximum. The mathematical formula for the normalization is: Normalized (x)=(x-min)/(max-min), where min and max are the minimum and maximum within the patient, respectively.

Data visualization
Figure 2, panels a-b were created with BioRender.com.

Institutional review board statement
Our studies were conducted in accordance with principles for human experimentation as defined in the U.S. Common Rule and were approved by the Human Investigational Review Board of each study center under Partners institutional review board (IRB)-approved protocol number 2017P001581. All healthy control subjects were screened for pertinent oncologic and neurologic medical histories. Individuals with a history of cancer, neurological disorders, and infectious diseases were excluded from the study.

Informed consent statement
All samples were collected with written informed consent after the patient was advised of the potential risks and benefits, as well as the investigational nature of the study.

Reporting summary
Further information on research design is available in the Nature Portfolio Reporting Summary linked to this article.

Data availability
The ddPCR data generated in this study are provided in the Supplementary Information and Source Data file. The raw ddPCR The ddPCR 1-dimensional (1D) and 2-dimensional (2D) plots are not publicly available, but they are available upon request from the corresponding author. The raw data (Supplementary Tables. 2,3) of individual replicates in the form of copy number is provided. Source data are provided with this paper.

References

1. Lin, D. et al. Trends in Intracranial Glioma Incidence and Mortality in the United States, 1975–2018. *Front. Oncol.* **11**, 748061 (2021).
2. Yan, H. et al. IDH1 and IDH2 mutations in gliomas. *N. Engl. J. Med.* **360**, 765–773 (2009).
3. Dang, L. et al. Cancer-associated IDH1 mutations produce 2-hydroxyglutarate. *Nature* **462**, 739–744 (2009).
4. Nobusawa, S., Watanabe, T., Kleihues, P. & Ohgaki, H. IDH1 mutations as molecular signature and predictive factor of secondary glioblastomas. *Clin. Cancer Res* **15**, 6002–6007 (2009).
5. Hertler, C. et al. Long-term survival with IDH wildtype glioblastoma: first results from the ETERNITY Brain Tumor Funders' Collaborative Consortium (EORTC 1419). *Eur. J. Cancer* **189**, 112913 (2023).
6. Hooper, G. W., Ansari, S., Johnson, J. M. & Ginat, D. T. Advances in the radiological evaluation of and theranostics for glioblastoma. *Cancers* **15**, 4162 (2023).
7. Katzendobler, S. et al. Diagnostic yield and complication rate of stereotactic biopsies in precision medicine of gliomas. *Front. Neurol.* **13**, 822362 (2022).
8. van den Bent, M. J. Interobserver variation of the histopathological diagnosis in clinical trials on glioma: a clinician's perspective. *Acta Neuropathol.* **120**, 297–304 (2010).
9. Zhu, P. et al. The detrimental effect of biopsy preceding resection in surgically accessible glioblastoma: results from the national cancer database. *J. Neurooncol.* **168**, 77–89 (2024).
10. Eibl, R. H. & Schneemann, M. Liquid biopsy and primary brain tumors. *Cancers* **13**, 5429 (2021).
11. Batool, S. M. et al. The Liquid Biopsy Consortium: challenges and opportunities for early cancer detection and monitoring. *Cell Rep Med* **4**, 101198 (2023).
12. Batool, S. M. et al. Extrinsic and intrinsic preanalytical variables affecting liquid biopsy in cancer. *Cell Rep Med.* **4**, 101196 (2023).
13. Muralidharan, K. et al. Promoter mutation analysis for blood-based diagnosis and monitoring of gliomas. *Clin. Cancer Res* **27**, 169–178 (2021).
14. Batool, S. M. et al. Highly sensitive EGFRvIII detection in circulating extracellular vesicle RNA of glioma patients. *Clin. Cancer Res* **28**, 4070–4082 (2022).
15. Figueroa, J. M. et al. Detection of wild-type EGFR amplification and EGFRvIII mutation in CSF-derived extracellular vesicles of glioblastoma patients. *Neuro. Oncol* **19**, 1494–1502 (2017).
16. Chen, W. W. et al. BEAMing and droplet digital PCR analysis of mutant IDH1 mRNA in glioma patient serum and cerebrospinal fluid extracellular vesicles. *Mol. Ther. Nucleic Acids* **2**, e109 (2013).
17. Louis, D. N. et al. The 2007 WHO classification of tumours of the central nervous system. *Acta Neuropathol.* **114**, 97–109 (2007).
18. Louis, D. N. et al. The 2016 World Health Organization classification of tumors of the central nervous system: a summary. *Acta Neuropathol.* **131**, 803–820 (2016).
19. Wen, P. Y. & Packer, R. J. The 2021 WHO classification of tumors of the central nervous system: clinical implications. *Neuro-oncology* **23**, 1215–1217 (2021).
20. Shen, G. et al. The MRI features and prognosis of gliomas associated With IDH1 mutation: a single center study in Southwest China. *Front. Oncol.* **10**, 852 (2020).
21. Joyner, D. A. et al. MRI features predict tumor grade in isocitrate dehydrogenase (IDH)-mutant astrocytoma and oligodendroglioma. *Neuroradiology* **65**, 121–129 (2023).
22. Cabezas-Camarero, S. et al. Detection of IDH1 mutations in plasma using BEAMing technology in patients with gliomas. *Cancers* **14**, 2891 (2022).
23. Boisselier, B. et al. Detection of IDH1 mutation in the plasma of patients with glioma. *Neurology* **79**, 1693–1698 (2012).
24. Husain, A., Mishra, S., Siddiqui, M. H. & Husain, N. Detection of IDH1 mutation in cfDNA and tissue of adult diffuse glioma with allele-specific qPCR. *Asian Pac. J. Cancer Prev.* **24**, 961–968 (2023).
25. Fujita, Y. et al. IDH1 p.R132H ctDNA and D-2-hydroxyglutarate as CSF biomarkers in patients with IDH-mutant gliomas. *J. Neurooncol.* **159**, 261–270 (2022).
26. Tuna, G. et al. Minimally invasive detection of IDH1 mutation with cell-free circulating tumor DNA and D-2-hydroxyglutarate, D/L-2-hydroxyglutarate ratio in gliomas. *J. Neuropathol. Exp. Neurol* **81**, 502–510 (2022).
27. Landers, M. J. F. et al. Oligodendrogliomas tend to infiltrate the frontal aslant tract, whereas astrocytomas tend to displace it. *Neuroradiology* **65**, 1127–1131 (2023).
28. Cancer Genome Atlas Research Network et al. Comprehensive, integrative genomic analysis of diffuse lower-grade gliomas. *N. Engl. J. Med.* **372**, 2481–2498 (2015).
29. DeWitt, J. C. et al. Cost-effectiveness of IDH testing in diffuse gliomas according to the 2016 WHO classification of tumors of the central nervous system recommendations. *Neuro. Oncol.* **19**, 1640–1650 (2017).

30. Bhaduri, A. et al. Outer radial glia-like cancer stem cells contribute to heterogeneity of glioblastoma. *Cell Stem Cell* **26**, 48–63.e6 (2020).
31. Neftel, C. et al. An integrative model of cellular states, plasticity, and genetics for glioblastoma. *Cell* **178**, 835–849.e21 (2019).
32. Tirosh, I. et al. Single-cell RNA-seq supports a developmental hierarchy in human oligodendroglioma. *Nature* **539**, 309–313 (2016).
33. Venteicher, A. S. et al. Decoupling genetics, lineages, and microenvironment in IDH-mutant gliomas by single-cell RNA-seq. *Science* **355**, eaai8478 (2017).
34. Nicholson, J. G. & Fine, H. A. Diffuse glioma heterogeneity and its therapeutic implications. *Cancer Discov.* **11**, 575–590 (2021).
35. Vij, M. et al. The prognostic impact of subclonal IDH1 mutation in grade 2-4 astrocytomas. *Neurooncol. Adv.* **5**, vdad069 (2023).
36. Carstam, L. et al. Long-term follow up of patients with WHO grade 2 oligodendroglioma. *J. Neurooncol.* **164**, 65–74 (2023).
37. Núñez, K. G. et al. Exosome shedding is concordant with objective treatment response rate and stratifies time to progression in treatment naïve, non-resectable hepatocellular carcinoma. *Livers* **3**, 727–738 (2023).
38. Andrade, L. N. et al. Extracellular vesicles shedding promotes melanoma growth in response to chemotherapy. *Sci. Rep.* **9**, 14482 (2019).
39. Gastpar, R. et al. Heat shock protein 70 surface-positive tumor exosomes stimulate migratory and cytolytic activity of natural killer cells. *Cancer Res.* **65**, 5238–5247 (2005).
40. Scholl, J. N. et al. Characterization and antiproliferative activity of glioma-derived extracellular vesicles. *Nanomedicine* **15**, 1001–1018 (2020).
41. Gromeier, M. et al. Very low mutation burden is a feature of inflamed recurrent glioblastomas responsive to cancer immunotherapy. *Nat. Commun.* **12**, 352 (2021).
42. Malta, T. M. et al. The epigenetic evolution of glioma is determined by the idh1 mutation status and treatment regimen. *Cancer Res.* **84**, 741–756 (2024).
43. Choi, B. D. et al. Intraventricular CARv3-TEAM-E T cells in recurrent glioblastoma. *N. Engl. J. Med.* **390**, 1290–1298 (2024).

Acknowledgements

The authors would like to thank all the MGH Neurosurgery clinicians and staff who assisted with the collection of samples. We are also deeply appreciative to the patients and their families for participating in the study. This work is supported by grants U01 CA230697 (BSC, LB), and R01 CA239078, CA237500 (BSC, LB). MGN Transformative Scholar (LB), Rappaport Scholar (LB). The funding sources had no role in the writing of the manuscript or the decision to submit the manuscript for publication. The authors have not been paid to write this article by any entity. The corresponding author has full access and assumes final responsibility for the decision to submit for publication.

Author contributions

S.M.B., L.B., B.S.C.: Data curation, formal analysis, validation, investigation, visualization, writing—original draft, writing—review and editing. A.K.E., T.H., E.E., S.K., A.S.G., H.Z.: experimental work, analysis, review and editing. S.M.B., L.B., B.S.C., H.Z., J.S., J.M., A.O.S., D.C.: Formal analysis, methodology, review and editing. L.B., B.S.C.: Conceptualization, resources, data curation, software, formal analysis, supervision, funding acquisition, validation, investigation, visualization, methodology, writing—original draft, project administration, writing—review and editing.

Competing interests

L.B., B.S.C., S.M.B. are inventors in a pending patent application, "Multiplexing tumor specific blood-based assays" (patent number: MGH 2023-345). The remaining authors declare no competing interests.

Additional information

Supplementary information The online version contains supplementary material available at https://doi.org/10.1038/s41467-024-51332-7.

Correspondence and requests for materials should be addressed to Leonora Balaj.

Peer review information *Nature Communications* thanks Thuy Ngo who co-reviewed with Kenneth Riley and the other, anonymous, reviewer(s) for their contribution to the peer review of this work. A peer review file is available.